AIP | Review of Scientific Instruments

Single fiber Bragg grating sensor with two sections of different diameters for longitudinal strain and temperature discrimination with enhanced strain sensitivity

Samir K. Mondal, Umesh Tiwari, Gopal C. Poddar, Vandana Mishra, Nahar Singh, Subhash C. Jain, S. N. Sarkar, K. D. Chattoypadhya, and Pawan Kapur

Citation: Review of Scientific Instruments **80**, 103106 (2009); doi: 10.1063/1.3247900
View online: http://dx.doi.org/10.1063/1.3247900
View Table of Contents: http://scitation.aip.org/content/aip/journal/rsi/80/10?ver=pdfcov
Published by the AIP Publishing

Single fiber Bragg grating sensor with two sections of different diameters for longitudinal strain and temperature discrimination with enhanced strain sensitivity

Samir K. Mondal,[1,2] Umesh Tiwari,[1,2] Gopal C. Poddar,[1,2] Vandana Mishra,[1,2] Nahar Singh,[1,2] Subhash C. Jain,[1,2] S. N. Sarkar,[3] K. D. Chattoypadhya,[1,2] and Pawan Kapur[1,2]
[1]*Central Scientific Instruments Organisations, Sec.-30C, Chandigarh, India*
[2]*Council of Scientific and Industrial Research, New Delhi 110001, India*
[3]*Department of Electronic Science, University of Calcutta, 92-A.P.C Road, Kolkata 700 009, India*

(Received 16 July 2009; accepted 14 September 2009; published online 30 October 2009)

A single fiber Bragg grating (FBG) sensor with two sections of different diameters is proposed and experimentally demonstrated for discrimination and measurement of strain and temperature. A section of single FBG is etched in hydrofluoric acid solution to reduce diameter of the fiber by factor of $<1/2$ to increase its strain sensitivity. Different shifts of the Bragg wavelengths of chemically etched and nonetched gratings caused by different strain sensitivities are used to discriminate and measure strain and temperature. Maximum errors of $\pm 13\mu\varepsilon$ (microstrain) and ± 1 °C are reported over $1700\mu\varepsilon$ and 60 °C measurement ranges, respectively. Depending upon the diameter of the etched fiber grating, the design can also discriminate nanostrain from temperature. © *2009 American Institute of Physics.* [doi:10.1063/1.3247900]

I. INTRODUCTION

Fiber Bragg grating (FBG) has emerged as a promising sensing element owing to its potential for the measurement of several important physical parameters such as strain, temperature, pressure, etc.[1–6] FBG based sensors have received significant attention for applications in modern telecommunication and optical sensor networks.[7] It has several inherent advantages over conventional electrical sensor in view of its nonconductivity, fast response, and immunity to electromagnetic waves. The basic principle of FBG sensor is based on the shift of the Bragg wavelength caused by the modulation of gratings refractive index due to thermo-optic effect and strain effect. One of the technical issues is the inability of FBG sensor to separate wavelength shift produced from strain effect and temperature effect which are tangled to each other developing cross sensitivity effect. Accurate measurement of strain and temperature requires elimination of cross sensitivity effect. FBG sensor is becoming an integral part of smart structure health monitoring. A considerable number of techniques for temperature and strain discrimination involving FBG sensors has been proposed and demonstrated,[8–14] such as the hybrid FBG/long period fiber grating sensor,[4] superimposed FBGs sensor,[15] using birefringence effect in FBG,[6] etc. There is also another type of FBG based sensor that combines FBG with other technique, such as the FBG cavity sensor,[16] combined fluorescence lifetime decay and FBG technique,[17] extrinsic Fabry–Pérot interferometer combined with chirped in-FBG,[18] etc. One most simple technique could be implementing combination of two FBG of different fiber diameter. In Ref. 13, James *et al.* proposed a design by writing grating at the junction of two spliced fiber of slightly different diameters. The spliced FBGs have different thermal and strain sensitivities which make the strain temperature discrimination model complex. The analytical model of the design depends upon two variables of radius as well as length of the FBGs. Also, most FBG based sensors are devoted to strain and temperature discrimination and no effort is given on design for strain and temperature discrimination with enhanced strain sensitivity, which is usually 1/10th of the thermal sensitivity.

In this paper, we propose a single FBG sensor with two sections having significant difference in diameters and a simple analytical model for strain and temperature discrimination with enhanced strain sensitivity. The model is based on one variable of function of diameter of the fiber and it exploits different strain responses of the gratings due to large mismatch in diameters made by partial etching of the FBG in HF solution. The enhanced strain sensitivity should reduce the error in strain and temperature discrimination. The measured strain and temperature obtained experimentally using our model match closely with the applied values. The sensor also has potential to discriminate nano-order strain from temperature depending upon the reduced diameter of the etched part of the fiber.

The remaining part of the paper is organized as follows. Section II describes sensor design and principle. Section III presents experimental results and discussion on strain and temperature discrimination using the proposed model. Finally, a conclusion is drawn in Sec. IV.

II. SENSOR DESIGN AND PRINCIPLE

The design of the proposed FBG sensor is schematically shown in Fig. 1. A 5 cm long FBG is inscribed in a germanium doped photosensitive fiber using 248 nm ultraviolet laser assisted grating writing facility. The Bragg wavelength of the FBG is chosen as 1550.568 nm. A section, one half of

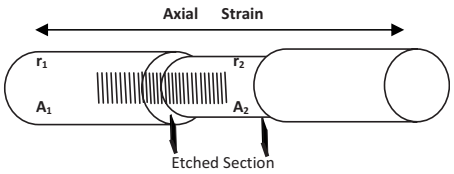

FIG. 1. Schematic diagram of the partially etched FBG sensor under longitudinal strain. (r_1,A_1) and (r_2,A_2) denote radius and area of cross sections of nonetched grating (FBG-1) and etched grating (FBG-2) fiber, respectively.

the length of the FBG, is etched in 48% HF solution to reduce its diameter. The diameter of the etched part is monitored by etching time with an etching rate of 3.1 μm/min at room temperature. The area of the cross sections of the nonetched and etched part are denoted by A_1 and A_2, respectively.

It is understood that the strain response of the grating in the etched part will be different from that of the nonetched part due to the difference in diameter in two sections. Therefore, the shift in center wavelengths for FBG-1 (Section-A_1) and FBG-2 (Section-A_2) due to change in longitudinal strains ($\Delta\varepsilon$) and temperatures (ΔT) can be expressed as[6]

$$\Delta\lambda_{B1} = \lambda_{B1}[\kappa_{T1}\Delta T + k_{\varepsilon 1}\Delta\varepsilon_1], \tag{1a}$$

$$\Delta\lambda_{B2} = \lambda_{B2}[\kappa_{T2}\Delta T + k_{\varepsilon 2}\Delta\varepsilon_2], \tag{1b}$$

where κ_{Ti} and $\kappa_{\varepsilon i}$ $(i=1,2)$ are the coefficients of thermal and strain sensitivities of the gratings and $\Delta\lambda_{B1}$, and $\Delta\lambda_{B2}$ are the shifts of Bragg wavelengths λ_{B1} and λ_{B2} for FBG-1 and FBG-2, respectively. As two gratings are part of same optical fiber, we take $k_{\varepsilon 1}$ and $k_{\varepsilon 2}$, and k_{T1} and k_{T2} are same for FBG-1 and FBG-2. It is known that the strain should vary with cross section of the fiber as $\Delta\varepsilon\alpha 1/\pi r^2$, r is the radius of the fiber. Therefore, one can propose a relation between longitudinal strains in two sections as

$$\frac{\Delta\varepsilon_1}{\Delta\varepsilon_2} = \frac{A_2}{A_1}, \tag{2}$$

where $A_1(=\pi r_1^2)$ and $A_2(=\pi r_2^2)$ denote area of circular cross sections for nonetched and etched fiber.

For strain and temperature discrimination, Eq. (1b) is subtracted from Eq. (1a) followed by substitution of Eq. (2) to separate strain response as

$$(\Delta\lambda_{B1} - \Delta\lambda_{B2}) = k_{\varepsilon 1}\left(1 - \frac{A_1}{A_2}\right)\Delta\varepsilon_1. \tag{3}$$

Equation (3) can be used to determine $\Delta\varepsilon_1$ for given diameters of the fiber in etched and nonetched sections and $k_{\varepsilon 1}$ provided the shifts $\Delta\lambda_{B1}$ and $\Delta\lambda_{B2}$ are found experimentally. The calculated strain value could be substituted in any of the Eq. (1a) or Eq. (1b) to determine temperature.

III. EXPERIMENTAL RESULTS AND DISCUSSION

As the working principle of the design based upon $\Delta\varepsilon\alpha 1/\pi r^2$, the relation between strain and radius of the FBG, we first present our experimental results on measuring strain response of FBG under an arbitrary load while reducing diameter of the fiber inscribed with Bragg grating to verify Eq. (2). The diameter of the fiber is continuously reduced by etching in HF solution. Figure 2 presents strain and Bragg wavelength shifts as a function of radius of the fiber with Bragg grating. The Bragg wavelength shift is noted during etching of the FBG in 48% HF solution. One end of the grating is connected to FBG interrogator to note wavelength shifts. The other end of the fiber carrying an arbitrary mass hangs inside a plastic tube containing acid solution. The plastic tube contains certain amount of commercial glycerin at the bottom of the tube. The HF solution is found to be lighter than glycerin and floats on glycerin inside the tube. The mass hanging from the end of the grating fiber remains inside the glycerin and, therefore, is unaffected by corrosive HF solution. Finally, etching rate is used to find the respective diameter during etching period. We also use same mass to theoretically calculate strain as a function of radius. The Young modulus (modulus of elasticity) of the fiber is taken as $Y=(7.18\times 10^{10}\ \mathrm{N/m^2})$ for theoretical strain calculation.[19] In Fig. 2, we observe an excellent match between the slopes of wavelength shift and microstrain for varying radius expecting their dependence by a linear function to each other and it justifies the validity of using Eq. (2) in our model. The inset of Fig. 2 shows extended theoretical plot of the strains as a function of the fiber radius and predicts the limit of the strain sensitivity of the design.

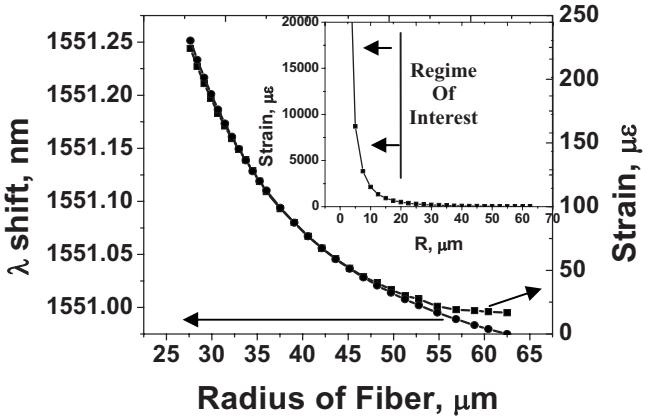

FIG. 2. Comparison of theoretical and experimental values of strain (in terms of wavelength shift) as a function of radius of the grating fiber. The inset is extended theoretical plot of strain as a function of radius of the fiber, $\Delta\varepsilon\alpha 1/\pi r^2$.

In our experiment for discrimination of strain and temperature, the FBG is stretched in between two holders of strain measuring station. Tension is induced to the FBG by applying tension in strain measuring station. Applied tension is measured through digital display monitor fitted with the station. Two ends of FBG are connected to an Optical Spectrum Analyzer, ANDO-6319 and light source, respectively. The fiber passes through a stand of aluminum channel which is being heated externally. A digital thermometer is attached with the Aluminum channel close to the FBG to read temperature of the grating. Wavelength shifts for FBG-1 ($\Delta\lambda_{B1}$) and FBG-2 ($\Delta\lambda_{B2}$) are noted with change in temperature and strains. Figure 3 is the optical spectrum showing wavelength shift characteristics of FBG-1 and FBG-2 under an arbitrary tension applied to the fiber at constant temperature $T=30$ °C.

It is observed that the Bragg wavelength, λ_{B2}, of etched

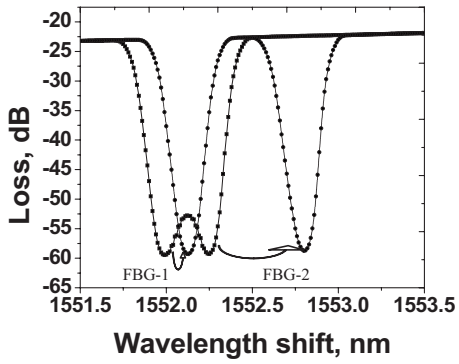

FIG. 3. Shift of two peaks under arbitrary tension. The peak for etched FBG-2 experiences approximately four times shift compared to nonetched FBG-1.

FBG-2 with fiber diameter of ~61.75 μm shifts by 355 pm (1552.799–1552.244 nm) compared to ~89 pm shift of λ_{B1} for FBG-1 with fiber diameter of 125 μm. The 3.97 (355/89) times shift is determined by the relation $\Delta\varepsilon_1/\Delta\varepsilon_2 = A_2/A_1(\sim 1/4)$, given by Eq. (2). The experimentally obtained shifts $\Delta\lambda_{B1}$ and $\Delta\lambda_{B2}$ for FBG-1 and FBG-2 are plotted in Fig. 4(a) as a function of strain at constant temperature. Another set of experiment is done on the sensor probe with $A_1/A_2 \sim 17$ and shifts of the center wavelengths of FBG-2 and FBG-1 are plotted in Fig. 4(b). Figure 4(b) also shows ~17 times more shift in the center wavelength of FBG-2 compared to that of FBG-1 as r_2 is $\sim 1/4$ of r_1(62.5 μm). The trend lines in Figs. 4(a) and 4(b) corresponding to wavelength shifts for FBG-2 have gradient 4 and 17.6 times more compared to that of the FBG-1 and deserve more strain sensitive behavior. During experiment, we

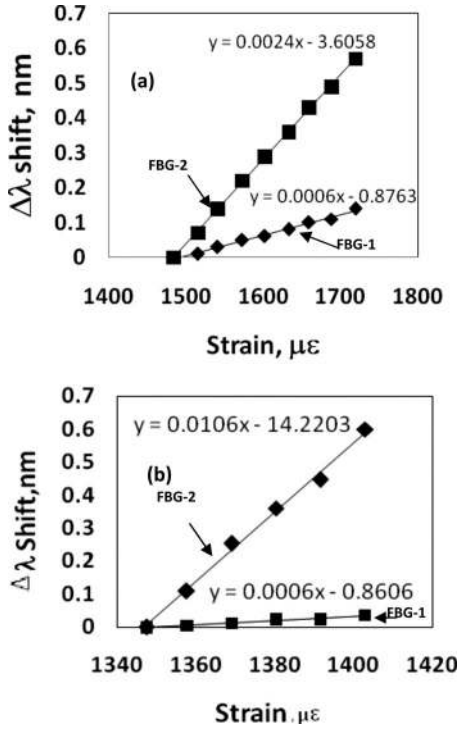

FIG. 4. Plots (a) and (b) compare wavelength shift for FBG-1 with the shift in FBG-2 of diameter 61.75 and 32 μm, respectively, as a function of strain.

TABLE I. Strain measurement in terms of resultant wavelength shift of FBG-1 and FBG-2 at fixed temperature $T=30$ °C. $\boldsymbol{\Delta\varepsilon_1}$ in first and fifth rows are the induced strain corresponding to applied load ΔW.

Initial weight (W=0.1275 kg)	T=30 °C ΔW=10.1 g ($\Delta\varepsilon_1=113\mu\varepsilon$)	T=30 °C ΔW=15.2 g ($\Delta\varepsilon_1=172\mu\varepsilon$)	T=30 °C ΔW=20.1 g ($\Delta\varepsilon_1=226\mu\varepsilon$)
λ_{B1}(nm)	λ_{shift1}(nm)	λ_{shift1}(nm)	λ_{shift1}(nm)
1551.850	1551.920	1551.950	1551.990
(Grating-A_1)	$\Delta\lambda_{B1}$=70 pm	$\Delta\lambda_{B1}$=100 pm	$\Delta\lambda_{B1}$=140 pm
λ_{B2}(nm)	λ_{shift2}(nm)	λ_{shift2}(nm)	λ_{shift2}(nm)
1552.090	1552.380	1552.520	1552.660
(Grating-A_2)	$\Delta\lambda_{B2}$=290 pm	$\Delta\lambda_{B2}$=430 pm	$\Delta\lambda_{B2}$=570 pm
Measured[a]	220 pm	330 pm	430 pm
($\Delta\lambda_{B1}-\Delta\lambda_{B2}$) and $\Delta\varepsilon_m$	$\Delta\varepsilon_m$=122.2$\mu\varepsilon$	$\Delta\varepsilon_m$=183$\mu\varepsilon$	$\Delta\varepsilon_m$=238.8$\mu\varepsilon$
Applied[b]			
$\Delta\varepsilon_1$ and	$\Delta\varepsilon_1$=113$\mu\varepsilon$	$\Delta\varepsilon_1$=172$\mu\varepsilon$	$\Delta\varepsilon_1$=226$\mu\varepsilon$
($\Delta\lambda_{B1}-\Delta\lambda_{B2}$)	203.4 pm	309.6 pm	406.8 pm

[a]($\Delta\lambda_{B1}-\Delta\lambda_{B2}$), known from the experiment, is put in Eq. (3) to find $\Delta\varepsilon_m$.
[b]$\Delta\varepsilon_1$, known from applied weight, is put in Eq. (3) to find ($\Delta\lambda_{B1}-\Delta\lambda_{B2}$). We use k_ε=0.6 pm/$\mu\varepsilon$ and A_1/A_2=4 to calculate ($\Delta\lambda_{B1}-\Delta\lambda_{B2}$) and $\Delta\varepsilon_m$.

change relative loads by 2.5 g and 5 mg in steps for the probes with A_1/A_2=4 and 17, respectively, while temperature is changed between 25 and 60 °C in step of ΔT=5 °C. The wavelength shifts for FBG-1 (λ_{B1}) and FBG-2 (λ_{B2}) are noted during variation of loads and temperature. The strain sensitivity (k_ε) for FBG-1 is obtained as 0.6 pm/$\mu\varepsilon$. The value of A_1/A_2, k_ε, and $\Delta\lambda_{B1}$ and $\Delta\lambda_{B2}$ are used in Eq. (3) for calculating applied strain which is substituted in Eq. (1a) to determine temperature.

Table I gives an example of how to extract information about arbitrarily applied strain. The applied weight (ΔW) is converted to applied strain $\boldsymbol{\Delta\varepsilon_1}$ (in first row) using stress-strain relation with Young's modulus of optical fiber for comparison with the measured strain, $\boldsymbol{\Delta\varepsilon_m}$, obtained from the model. The measured strains $\boldsymbol{\Delta\varepsilon_m}$ in the fourth row are obtained by fitting experimentally obtained ($\Delta\lambda_{B1}-\Delta\lambda_{B2}$) into Eq. (3) for known value of A_1/A_2=4 and k_ε =0.6 pm/$\mu\varepsilon$.

Values of expected ($\Delta\lambda_{B1}-\Delta\lambda_{B2}$) for applied strains $\Delta\varepsilon_1$ are given in *italics* in the fifth row. $\Delta\lambda_{B1}$ and $\Delta\lambda_{B2}$ are the Bragg wavelength shift obtained experimentally while strain and temperature are changed simultaneously. The other strains with varying temperature are similarly calculated and plotted in Fig. 5.

Figure 5 experimentally compares measured strains with the applied strains. Figures 5(a) and 5(b) correspond to $A_1/A_2 \sim 4$ and 17, respectively. The half-filled circles on dotted straight lines are applied strains at different temperature, while the empty circle point nearest to the half-filled circle point is the respective measured value of the strain. The errors in two cases are within ± 13 and $\pm 7\mu\varepsilon$ over ranges of $1700\mu\varepsilon$ and $1400\mu\varepsilon$, respectively. We also measured temperature using applied strains in strain–temperature relation given in Eq. (1) and the temperature sensitivity 8 pm/°C (found from the experiment) of the FBG. The measured temperature closely matches with applied temperature with maximum error of ±1 °C over 60 °C range.

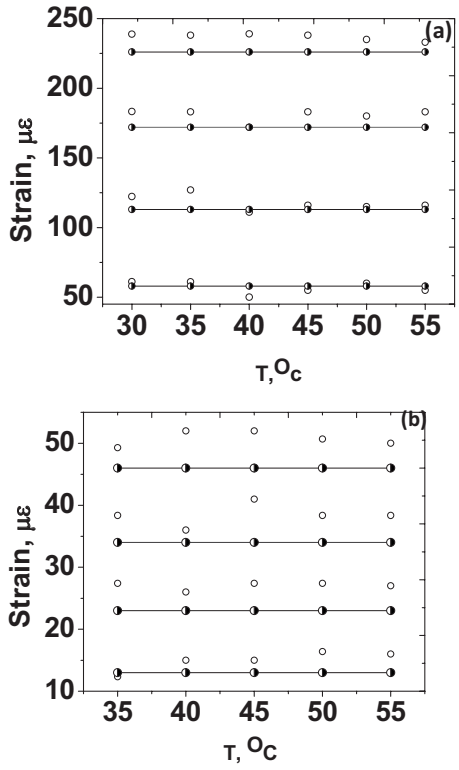

FIG. 5. Comparison between applied and measured strains by the proposed model. The half-filled circle points on solid lines are applied strain at different temperature. The empty circle point nearest to the half-filled circle point is the respective strain obtained from the model.

IV. CONCLUSION

We propose a single FBG with two sections of different diameters to discriminate strain and temperature. The analytical model for the sensor is simple and depends upon the radius of the fiber only. We experimentally demonstrated the proposed sensor for strain and temperature discrimination. The values of the strains and temperature obtained from our model match closely with the applied values. Maximum errors of $\pm 13 \mu\varepsilon$ and ± 1 °C are obtained over the range of $1700 \mu\varepsilon$ and 60 °C temperature, respectively. The sensor could be made highly strain sensitive by reducing diameter of the etched section and thus it is possible to measure nano-order strain including temperature discrimination. The design could be useful for strain and temperature discrimination in structural health monitoring as well as nano-order strain measurement.

ACKNOWLEDGMENTS

The authors thank Dr. H. S. Maiti, Chairman, CSIR Task Force on Photonics for Laser, Communication and Sensor Technology, for the motivation and support for this work carried out under the CSIR Network Project.

[1] A. D. Kersey, M. A. Davis, H. J. Patrick, M. LeBlanc, K. P. Koo, C. G. Askins, M. A. Putnam, and E. J. Friebele, J. Lightwave Technol. **15**, 1442 (1997).
[2] Y. J. Rao, Meas. Sci. Technol. **8**, 355 (1997).
[3] K. Tian, Y. Liu, and Q. Wang, Opt. Fiber Technol. **11**, 370 (2005).
[4] H. J. Patrick, G. M. Williams, A. D. Kersey, J. R. Pedrazzani, and A. M. Vengsarkar, IEEE Photonics Technol. Lett. **8**, 1223 (1996).
[5] Y. S. Hsu, L. Wang, W.-F. Liu, and Y. J. Chiang, IEEE Photonics Technol. Lett. **18**, 874 (2006).
[6] S. T. Oh, W. T. Han, U. C. Paek, and Y. Chung, Opt. Express **12**, 724 (2004).
[7] M. D. Todd, G. S. Jhonson, and S. T. Vohra, Smart Mater. Struct. **10**, 534 (2001).
[8] O. Frazao, R. Romero, F. M. Araujo, L. A. Ferreira, and J. L. Santos, Sens. Actuators, A **120**, 490 (2005).
[9] J. Echevarria, A. Quintela, C. Jauregui, and J. M. Lopez-Higuera, IEEE Photonics Technol. Lett. **13**, 696 (2001).
[10] B. Guan, H. Tam, S. Ho, W. Chung, and X. Dong, Electron. Lett. **36**, 1018 (2000).
[11] O. Frazão, J. P. Carvalho, L. A. Ferreira, F. M. Araújo, and J. L. Santos, Meas. Sci. Technol. **16**, 2109 (2005).
[12] S. K. Mondal, V. Mishra, U. Tiwari, G. C. Poddar, N. Singh, S. C. Jain, S. N. Sarkar, and P. Kapur, Microwave Opt. Technol. Lett. **51**, 1621 (2009).
[13] S. W. James, M. L. Dockney, and R. P. Tatam, Electron. Lett. **32**, 1133 (1996).
[14] L. Xiaohong, W. Dexiang, Z. Fujun, and D. Enguang, Microwave Opt. Technol. Lett. **43**, 478 (2004).
[15] M. G. Xu, J.-L. Archambault, L. Reekie, and J. P. Dakin, Electron. Lett. **30**, 1085 (1994).
[16] W. C. Du, X. M. Tao, and H. Y. Tam, IEEE Photonics Technol. Lett. **11**, 105 (1999).
[17] S. A. Wade, D. I. Forsyth, K. T. V. Grattan, and Q. Guofu, Rev. Sci. Instrum. **72**, 3186 (2001).
[18] R. Yun-Jiang, Z. Xiang-Kai, Z. Yong, W. Yi-Ping, Z. Tao, R. Zeng-Ling, Z. Lin, and I. Bennion, Chin. Phys. Lett. **18**, 643 (2001).
[19] F. Pigeon, S. Pelissier, A. Mure-Ravaud, H. Gagnarie, and C. Veillas, Electron. Lett. **28**, 1034 (1992).